NANO LETTERS

2007
Vol. 7, No. 8
2435−2440

Individual Multiwall Carbon Nanotubes Spectroscopy by Scanning Transmission X-ray Microscopy

Alexandre Felten,*,† Carla Bittencourt,‡ Jean-Jacques Pireaux,† Manuela Reichelt,§ Joachim Mayer,§ Daniel Hernandez-Cruz,|| and Adam P. Hitchcock||

LISE, University of Namur, 61 rue de Bruxelles, 5000 Namur, Belgium, Materia Nova, Parc Initialis, Av. Nicolas Copernic 1, Mons 7000, Belgium, GFE, RWTH Aachen University, Ahornstrasse 55, 52074 Aachen, Germany, and Brockhouse Institute for Materials Research, McMaster University, Hamilton, Ontario L8S 4M1, Canada

Received May 15, 2007; Revised Manuscript Received June 16, 2007

ABSTRACT

Scanning transmission X-ray microscopy (STXM) has been used to probe the electronic structure of individual multiwall carbon nanotubes by chemical mapping at the nanoscale. Carbon 1s near-edge X-ray absorption fine structure (NEXAFS) spectra of individual structures are shown to be able to differentiate carbon nanotubes from onionlike carbon nanoparticles and to differentiate nanotubes synthesized by different growth methods. Imaging of the very same region by both STXM and transmission electron microscopy is shown to be a very useful and complementary approach.

In recent years, much progress has been made in the synthesis of carbon nanotubes driven by the high interest in the intrinsic properties of this material such as their nanometric cross section, high aspect ratio, and good thermal and electric conductivity, which points to many potential applications.[1−3] While carbon nanotube synthesis has been highly optimized, the study of their electronic properties is still lacking. Difficulties in the determination of the electronic properties of the CNTs, as in other nanostructures, arise from constraints associated with the poor spatial resolution of most of the available analytical techniques. Earlier electronic structure studies employed mainly nonspatially resolved near-edge X-ray absorption fine structure spectroscopy (NEXAFS)[4−6] and photoelectron spectroscopy (PES).[7−9] These spectroscopy techniques typically sample an area of some mm^2. Consequently, the electronic structure information they provided is an average over a large area in which a signal from impurities (amorphous carbon, onionlike particles, and catalysts) cannot be avoided. Besides this, a bundle of CNTs is always composed by several sorts of CNTs whose electronic properties can vary from metallic to semiconducting depending on their helicity and diameter as well as, in principle, on their mutual arrangement.

In contrast, techniques based on spectromicroscopy, such as transmission electron microscopy (TEM) equipped with electron energy loss spectroscopy (EELS)[10] and scanning photoemission microscopy (SPEM),[11−13] have been used for the analysis of selected zones or isolated carbon nanotubes. However, the spatial resolution of SPEM is at best 90 nm,[11] which makes it a challenge to measure isolated CNT structures. While TEM-EELS does provide very high spatial resolution, two other problems exist. Much more radiation damage is produced by an electron beam relative to a photon beam[14] and the energy resolution of conventional TEM-EELS instruments is significantly lower than that of synchrotron-based X-ray spectromicroscopy.[15−17] The latter technique thus offers a great potential not just for CNTs but for nanostructures in general. The improvements in the spatial resolution compared to classical X-ray absorption spectroscopy provide access to unique and important properties of isolated nanostructures that will have decisive impact in the nanotechnology era.

Here we demonstrate the power of scanning transmission X-ray microscopy (STXM)[15−17] to study the electronic and structural properties of carbon nanotubes. STXM combines both NEXAFS spectroscopy and microscopy with a spatial resolution better than 40 nm. NEXAFS spectroscopy[18] is a particularly well-adapted probe of carbon nanotubes,[4−6] as it is able to investigate both electronic and structural properties of carbon-based systems and can provide unique information about the composition of organic materials, as

* Corresponding author. E-mail: alexandre.felten@fundp.ac.be. Telephone: 0032(0)81725232. Fax: 0032(0)81724595.
† LISE, University of Namur.
‡ Materia Nova.
§ GFE, RWTH Aachen University.
|| Brockhouse Institute for Materials Research, McMaster University.

10.1021/nl071134e CCC: $37.00
Published on Web 07/11/2007

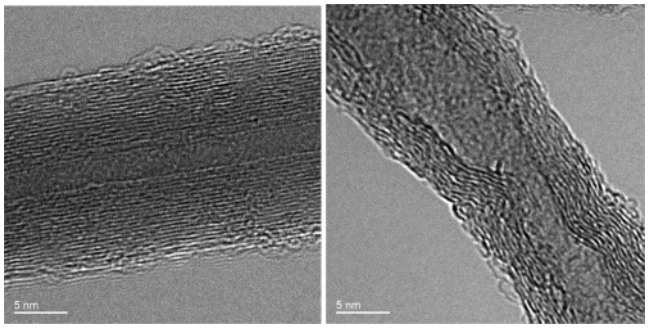

Figure 1. HRTEM pictures of MWCNT synthesized by arc-discharge (left) and CVD (right).

it can easily differentiate bonding types for carbon, oxygen, and nitrogen.[13] Here we show that this synchrotron-based spectromicroscopy technique is able to differentiate between the electronic states of multiwall carbon nanotube (MWCNTs) synthesized by arc-discharge or chemical vapor deposition (CVD) in addition to imaging one isolated MWCNT.

CVD and arc-discharge-synthesized MWCNTs are well known to have different crystallinity due to their different growth mechanisms.[19] Figure 1 shows high-resolution electron microscopy (HREM) images of MWCNTs synthesized by arc-discharge (Figure 1, left) and CVD (Figure 1, right). It can be seen that the arc-discharge CNTs are highly crystalline, with regular graphene sheets at an interlayer spacing of 3.4 Å, while the graphene layers of the CVD MWCNTs are not uniformly arranged. The curvature of the CNTs induces the redistribution of the electron density,[20] consequently, nonuniformities in the graphene layers are expected to be revealed by an increase in the line width of the carbon 1s $\rightarrow \pi^*$ NEXAFS line. The actual composition of the MWCNT powder is another important point that has to be considered in CNT studies. Powder produced by CVD typically contains 95% CNTs, while powder synthesized by arc-discharge consists of 40% of CNTs and the rest is impurities such as multilayer polygonal carbon nanoparticles (CNPs) and graphitic particles. Differences in the X-ray spectra and thus electronic structure of multiwall carbon nanotubes and carbon nanoparticle impurities will be shown to demonstrate the sensitivity of STXM-NEXAFS. The spectra of carbon nanoparticle impurities, pristine arc-discharge, and CVD-grown MWCNTs are compared, underlining the unique spectroscopic insights provided by STXM. The results obtained in this study open new possibilities for understanding the electronic and structural properties of individual carbon nanotubes and show the ability of STXM to perform nanostructure analysis.

To perform this work, carbon nanotube powders were purchased from Mercorp (arc-discharge grown)[21] and Nanocyl (chemical vapor deposition (CVD) grown).[22] The raw powders were sonically dispersed in ethanol, and a drop of the solution deposited on a holey Formvar TEM grid.[23] An important step to perform STXM measurements is a pre-analysis of the samples by TEM (see Figures 2b, 5b, 6b). If grids with labeled regions are used, location of individual carbon nanotubes can be identified before using synchrotron radiation resources and then the suitable region for analysis

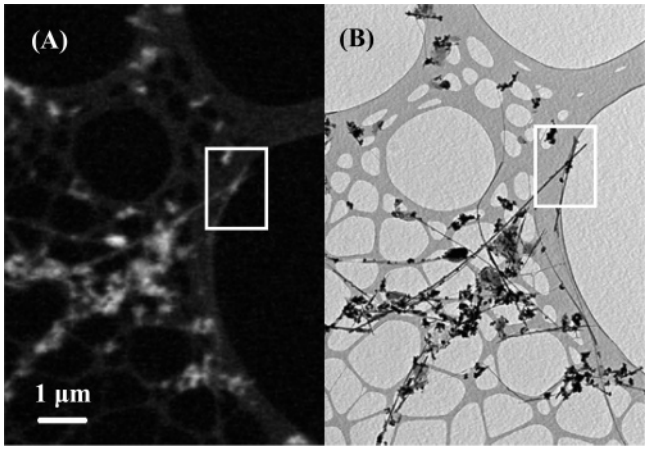

Figure 2. (A) STXM image of CNT powder deposited on a holey carbon-coated TEM grid. (B) TEM image of the same region.

can be easily retrieved; this is a time-saving step. Moreover, TEM study also gives information about the constituent of the raw powder as well as on the structure of the carbon nanotubes. Minimal dose TEM techniques were used to prescreen sample areas for STXM. As can be seen from Figure 2, the arc-discharge powder includes a large proportion of impurities in the form of amorphous and onionlike particles. The carbon nanotubes formed during the process are very straight and have a nearly perfect graphitic structure. Their diameters range from a few to a maximum of 50 nm. In contrast, the CVD powder consists mainly of multiwall carbon nanotubes that are bent, with no uniform walls, and their surface is covered by an amorphous carbon layer (Figure 1). The HRTEM pictures of Figure 1 have been taken using a Tecnai F20 operating at 200 kV. For the rest of the work, transmission electron microscopy was carried out on a Tecnai 10 microscope operating in low-dose conditions (80 kV) in order to prevent radiation damage of the specimens.

To perform the STXM analysis, the grid is fixed on a sample holder and inserted in the experimental chamber of the dedicated STXM[24] on beamline 5.3.2 at the Advanced Light Synchrotron at the Lawrence Berkeley National Laboratory.[25] The chamber is evacuated and then filled with a third of an atmosphere of helium. The monochromated X-ray beam is focused to a 40 nm spot on the sample using a Fresnel zone plate. The transmitted signal is then measured with single-photon counting using a phosphor converter and a high-performance photomultiplier tube. The energy resolution of the beamline is 150 meV and the spatial resolution is 40 nm with the zone plates used (155 μm diameter, 35 nm outer zones). The energy scale is calibrated using the C 1s $\rightarrow$ 3s transition of CO_2 (gas).

STXM can be used in three different acquisition modes. It is possible to acquire images at a specific photon energy, to acquire spectra at points or along lines, and to acquire a sequence of images over a range of photon energies (a "stack").[26] Stacks can be further processed and a quantitative chemical map of the analyzed region can be built up by fitting the spectrum of each pixel to a set of suitable reference spectra, which can be placed on quantitative intensity scales.

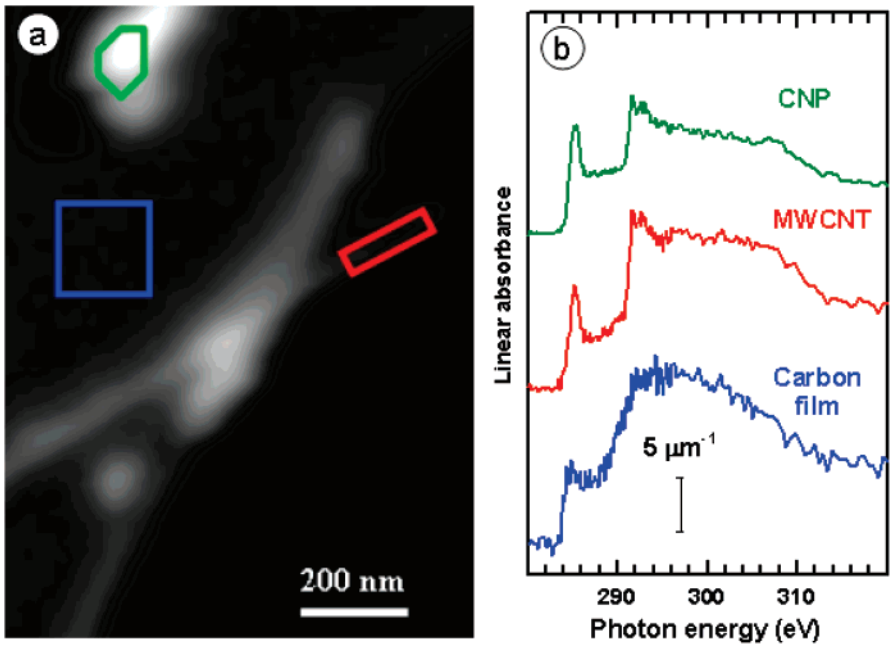

Figure 3. (a) Average of 200 STXM images (280−320 eV) in the region around one isolated arc-discharge-grown carbon nanotube. (b) NEXAFS spectra of the colored regions, placed on a quantitative linear absorbance scale by matching to elemental carbon (see text).

In this work, C 1s stacks were recorded with pixel size of 20 nm and dwell time (counting period at each pixel) of 1.2 ms. All STXM results were analyzed using aXis2000.[27] It is also worth noting that, for the clarity of the presentation, the results presented here are shown only for one particular sample, but the authors have carried out analysis of several similar samples with the same results as given.

A STXM analysis of a MWCNT powder synthesized by arc-discharge is shown in Figure 2. The TEM image (Figure 2b) shows that the powder mainly contains bundles of straight nanotubes and impurities. In addition, isolated multiwall carbon nanotubes can also be observed with a few lying on top of holes in the carbon support film. These isolated MWCNTs are the ones of interest for STXM analysis. Figure 2a shows a STXM image recorded at 291.7 eV, which is the energy of the 1s → σ^* transition in sp^2 hybridized C atoms. The very same region was imaged using an 80 kV TEM (Figure 2b). A closer look at this region reveals that an isolated multiwall carbon nanotube (MWCNT) can be seen; a magnified view is displayed in Figure 3. The diameter of this MWCNT is 41 nm.

Figure 3 displays the average of 200 STXM images acquired as an image sequence (stack)[26] between 280 and 320 eV on the region marked by a white square in Figure 2. In the right panel, C 1s NEXAFS spectra extracted from different areas of the stack are shown. The curves correspond to C 1s spectra recorded on the carbon film that covers the TEM grid (blue), the isolated multiwall carbon nanotube (red), and the carbon nanoparticles (green). The C 1s spectrum of the individual MWCNT is very similar to the spectrum reported for highly oriented pyrolitic graphite.[6,28] It is characterized by a sharp peak at 285.2 eV, which corresponds to the 1s → π^* transition in sp^2 hybridized C atoms and also by a broader peak at 291.7 eV, which is the 1s → σ^* resonance.

The spectra recorded on the carbon nanoparticles (CNP) exhibit the same features at 285.2 and 291.7 eV. However, the π^* peak of the CNP spectrum is broader (full width at half-maximum (fwhm) of 1.4 ± 0.05 eV) than that for the π^* peak of the isolated MWCNT (fwhm of 1.0 ± 0.05 eV). In addition, the region between 287 and 290 eV has a higher intensity, which is attributed to the presence of hydrogenated carbon atoms[29,30] in the particles as well as to oxygen adsorbed on the CNP.[28,31] These spectral differences illustrate the capability of STXM spectromicroscopy to differentiate nanostructures with quite similar electronic structures.

Stacks can be further processed to derive quantitative maps of the chemical components in the analyzed region by fitting the spectrum of each pixel to a set of suitable reference spectra.[27] This provides compositional information at the scale of individual pixels. It is one of the key aspects of the technique: STXM can perform not only elemental mapping but also quantitative chemical mapping with a spatial resolution below 50 nm.[32]

Figure 4 shows quantitative chemical maps of the three different forms of carbon present in the sample. These images are obtained by fitting the C 1s stack to spectra of the three components (Figure 3b), which were placed on quantitative linear absorbance scales (optical density per nm of material) by matching the intensities outside the structured C 1s absorption region to that for elemental carbon.[33] Further details on the quantitative mapping procedure can be obtained in refs 34,35. The gray scale of each component map gives the thicknesses in nanometers, assuming a density of the materials equal to 1.4 g/cm^3. A color composite map in which the three components are scaled using a common (0−88 nm) thickness scale is constructed to visualize their respective spatial distributions. Here the red, green, and blue colors correspond to the spatial distributions of MWCNT, onionlike

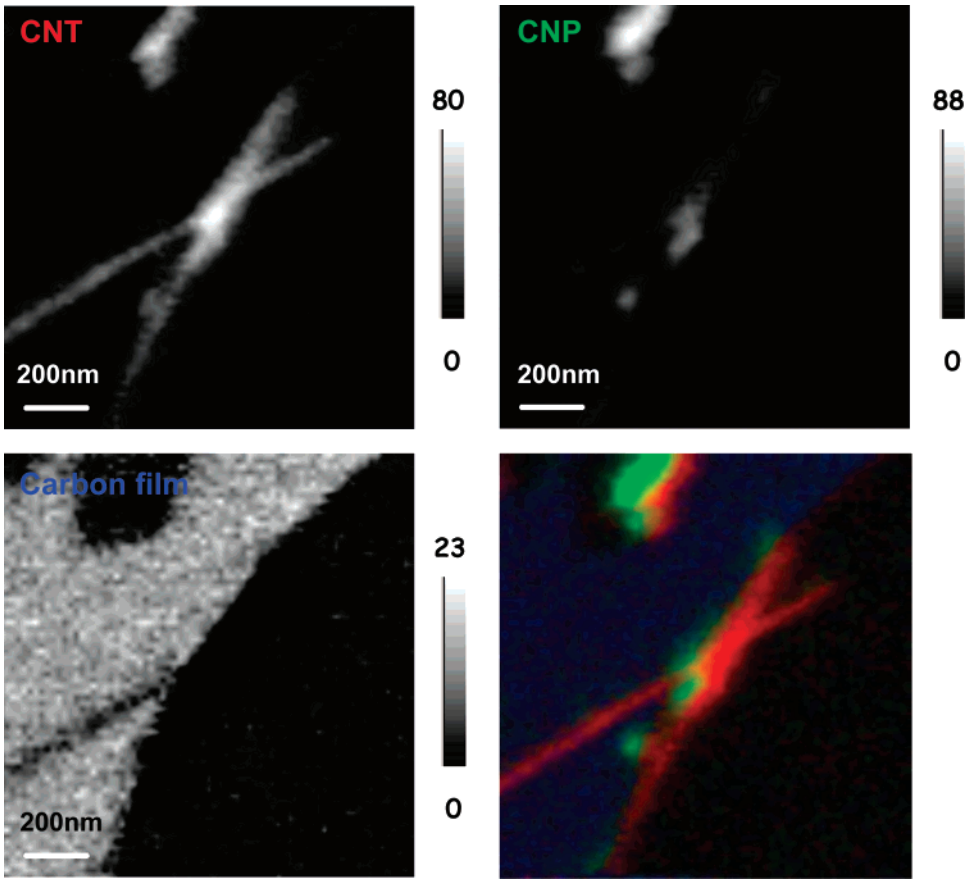

Figure 4. CNT, CNP, and carbon film quantitative chemical maps derived from the C 1s stack. The gray scales for each component are given in nm. A colored composite map is also included with a single thickness scale (0−88 nm) for all three components/colors.

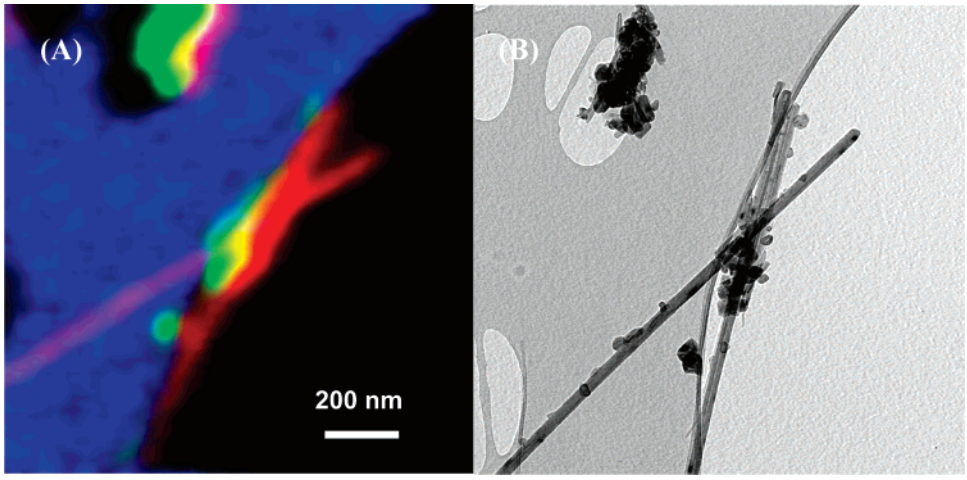

Figure 5. (A) Composite map of the same region as in Figures 3 and 4. The red, green, and blue colors correspond respectively to nanotube, carbon nanoparticles, and carbon grid rich region, and the components have been rescaled to fill each color dimension. (B) Corresponding TEM image.

carbon particles, and the carbon film, respectively. The carbon film in blue is difficult to see because it is much thinner than the other two components. From these maps, two carbon nanotubes are seen to be crossing in the center of the image and there are some nanoparticles lying at the intersection of the two nanotubes. A thicker group of CNPs (88 nm) is also observed at the top of the picture. The carbon film is estimated to be around 20 nm thick.

By carefully comparing, in Figure 5, the enhanced STXM composite image with the corresponding TEM image of the very same region, it can be seen that the colors perfectly match the locations of the nanoparticles and the nanotubes. It is important to point out that this approach can be used to differentiate between regions containing objects with signals as close as carbon nanotubes and onionlike carbon nanoparticles.

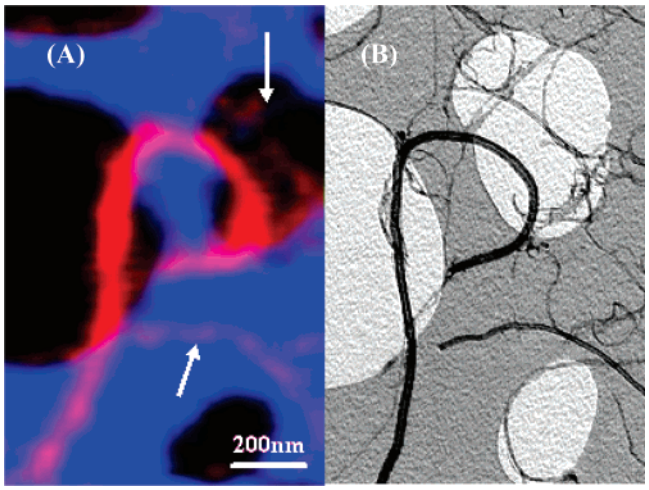

Figure 6. (A) Composite map of a region around a CVD-grown carbon nanotube. The red and blue colors correspond respectively to carbon nanotube and carbon grid rich regions. (B) Corresponding TEM image.

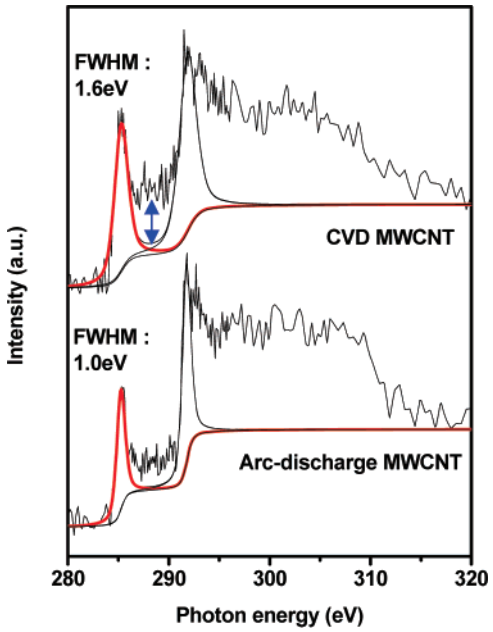

Figure 7. Comparison between NEXAFS spectra of isolated carbon nanotubes produce by arc-discharge and CVD method. The corresponding TEM images of these two nanotubes are shown in Figures 5 and 6.

Figure 6 shows the results of a STXM C 1s analysis of the CVD MWCNTs. From the TEM image (Figure 6b), it can be observed that the carbon nanotube diameters range from 10 to 36 nm. No carbon nanoparticles are present in this sample. The chemical map (Figure 6a) is a composite in which the nanotubes are red and the carbon film is blue. In addition to the large isolated MWCNT that can be observed at the center of the image, there are two other smaller features worth noting: a 20 nm nanotube that is clearly resolved (lower arrow), and a very small section of the carbon film that is among a set of thin MWCNTs (upper arrow). Nevertheless, for such small features, the spectral signal in a pixel will contain a non-negligible intensity from the surrounding material which affects sensitivity and at the limit does not allow one to cleanly identify smallest structures from their spectral intensity.

Regions containing individual carbon nanotubes were thus successfully imaged with high spatial resolution. Nevertheless, one of the main advantages of the STXM technique arises from the combination of both high spatial and high-energy resolution. This is further demonstrated by comparing two very similar nanostructures, i.e., arc-discharge and CVD synthesized nanotubes. Figure 7 compares NEXAFS spectra of both types of nanotubes. The analysis of the spectra is performed using a Shirley background in addition to two mixed Gaussian/Lorentzian functions for π^* and σ^* edges. The width of the C 1s $\rightarrow \pi^*$ peak in the two samples is first compared. It has been shown that this broadening is closely related with the amount of defect structure within the nanotubes.[36] A qualitative measure of the degree of imperfection of the nanotube structure can therefore be deduced by measuring the width of the carbon π^* peak. The full width at half-maximum (fwhm) of the arc-discharge MWCNT imaged in Figure 5 is 1.0 eV, which is very similar to that of graphite (reported to be 0.93 eV in ref 6 and 1.0 eV in ref 36). This reflects the fact that large-diameter arc-discharge multiwall carbon nanotubes have a structure very close to that of graphite. In contrast, the fwhm of the C 1s $\rightarrow \pi^*$ peak of the CVD nanotube (Figure 6) is 1.6 eV, much larger than that for the arc-discharge MWCNTs. This indicates that the nanotubes prepared by CVD are far from perfect and thus have large amounts of defects. Larger values for the FWHMs of C 1s $\rightarrow \pi^*$ peaks of carbon nanotubes have been reported by other groups (from 1.8 to 2.3 eV; measured with an energy resolution of 100 meV).[36] The higher values reported in that work could reflect physical differences in nanotubes prepared by a different method (grown ex situ on silicon wafer by thermal vapor deposition), but it may also reflect the fact that the spectrum was acquired over a large area (1 mm $\times$ 0.9 mm) which introduces contributions to the peak width from a broad distribution of nanotubes of different diameters and also probably different amounts of defects as well as from carbon impurities. Moreover, it has been reported that interaction among CNTs can also influence their electronic structure, which could also lead to broadening of the π^* peak.

In addition to the broadening of the C 1s $\rightarrow \pi^*$ peak, the intensity between 287 and 290 eV is much higher in the spectrum recorded on the CVD nanotubes. The signal in this energy range was reported to be associated with CH_x bonds as well as adsorbed oxygen.[29−31] Consequently, it indicates that amorphous carbon and defects are present at the surface of the CVD nanotube as the perfect CNT surface is expected to be nonreactive.[37] This is confirmed by the HREM image in Figure 1, which shows the presence of an amorphous layer on the CVD MWCNT.

In conclusion, we can say that electronic properties of carbon nanotubes have been probed at the nanoscale using STXM. The spatial resolution of the technique enables the study of individual carbon nanotubes by avoiding contributions from other components of the raw powder, while the high-energy resolution allows differentiation among very

similar nanostructures, i.e., MWCNTs synthesized by two different methods, through sensitivity to quite subtle differences in the NEXAFS spectra (peak widths and weak features). Examination of the very same area by TEM is shown to be a very useful approach that, when combined with the spatially resolved NEXAFS spectra recorded by STXM image sequences, leads to unambiguous identification of all objects present in the region analyzed. We expect that combined TEM, STXM studies will provide advantages to the study of other nanostructures. In this general context, it is important to note that the rate of radiation damage relative to analytical signal is 100−1000 times smaller for STXM than for TEM-EELS.[14] This, as well as the ability to study fully hydrated samples (soft X-rays in the C 1s region penetrate 5 μm of water, with a residual transmission of 5% at 285 eV), mean the technique is applicable to study nanostructures in the context of environmental[38−41] and biological[15,38−42] applications.

Acknowledgment. This work was supported by the Région Wallone (Enable project), PAI 5/1/1 on "Quantum Size Effects in Nanostructured Materials" (Belgium), the Nanobeams EU Network of Excellence, NSERC (Canada), and the Canada Research Chair program (A.P.H.). Construction and operation of the STXM 5.3.2 microscope is supported by NSF DMR, NSERC, and the Canada Foundation for Innovation. Zone plates were supplied by the Centre for X-ray Optics, LBNL. We thank A. L. D. Kilcoyne and T. Tyliszczak for their expert work in developing and maintaining STXM532. The Advanced Light Source is supported by the Director, Office of Energy Research, Office of Basics Energy Sciences, Materials Sciences Division of the U.S. Department of Energy, under contract no. DE-AC03-76SF00098.

References

(1) Robertson, J. *Mater. Today* **2004**, *7* (10), 46.
(2) Baughman, R. H.; Zakhidov, A. A.; de Heer, W. A. *Science* **2002**, *297*, 787.
(3) de Heer, W. A. *MRS Bull.* **2004**, *29*, 281.
(4) Hemraj-Benny, T.; Banerjee, S.; Sambasivan, S.; Balasubramanian, M.; Fischer, D. A.; Eres, G.; Puretzky, A. A.; Geohegan, D. B.; Lowndes, D. H.; Han, W.; Misewich, J. A.; Wong, S. S. *Small* **2006**, *2*, 26.
(5) Tang, Y. H.; Sham, T. K.; Yu, Y. F.; Lee, C. S.; Lee, S. T. *Chem. Phys. Lett.* **2002**, *366*, 636.
(6) Zhong, J.; Song, L.; Wu, Z. Y.; Xie, S.-S.; Abbas, M.; Ibrahim, K.; Qian, H. *Carbon* **2006**, *44*, 866.
(7) Larciprete, R.; Goldoni, A.; Lizzit, S.; Petaccia, L. *Appl. Surf. Sci.* **2005**, *248*, 8.
(8) Yoon, S. W.; Kim, S. Y.; Park, J.-Y.; Park, C. J.; Lee, C. J. *J. Phys. Chem. B* **2005**, *109*, 20403.
(9) Suzuki, S.; Watanabe, Y.; Kiyohura, T.; Nath, K. G.; Ogino, T.; Heun, S.; Zhu, W.; Bower, C.; Zhou, O. *Phys. Rev. B* **2001**, *63*, 245418.
(10) Stephan, O.; Kociak, M.; Henrard, L.; Suenaga, K.; Gloter, A.; Tencé, M.; Sandré, E.; Colliex, C. *J. Electron Spectrosc. Relat. Phenom.* **2001**, *114−116*, 209.
(11) Goldoni, A.; Larciprete, R.; Gregoratti, L.; Kaulich, B.; Kiskinova, Zhang, Y.; Dai, H.; Sangaletti, L.; Parmigiani, F. *Appl. Phys. Lett.* **2002**, *80*, 2165.
(12) Suzuki, S.; Watanabe, Y.; Ogino, T.; Homma, Y.; Takagi, D.; Heun, S.; Gregoratti, L.; Barinov, A.; Kiskinova, M. *Carbon* **2004**, *42*, 559.
(13) Chiou, J. W.; Yueh, C. L.; Jan, J. C.; Tsai, H. M.; Pong, W. F.; Hong, I.-H.; Klauser, R.; Tsai, M.-H.; Chang, Y. K.; Chen, Y. Y.; Wu, C. T.; Chen, K. H.; Wei, S. L.; Wen, C. Y.; Chen, L. C.; Chuang, T. J. *Appl. Phys. Lett.* **2002**, *81*, 4189.
(14) Rightor, E. G.; Hitchcock, A. P.; Ade, H.; Leapman, R. D.; Urquhart, S. G.; Smith, A. P.; Mitchell, G.; Fischer, D.; Shin, H. J.; Warwick, T. *J. Phys. Chem. B* **1997**, *101*, 1950.
(15) Kirz, J.; Jacobsen, C.; Howells, M. *Q. Rev. Biophys.* **1995**, *28*, 33.
(16) Ade, H. In *Experimental Methods In The Physical Sciences*; Academic Press: New York, 1998; Vol. 32, p 225.
(17) Ade, H.; Urquhart, S. G. In *Chemical Applications of Synchrotron Radiation*; World Scientific: River Edge, NJ, 2002; Vol. 12A, p 285.
(18) Stöhr, J. *NEXAFS Spectroscopy*; Springer-Verlag: New York, 2003.
(19) Thien-Nga, L.; Bonard, J.-M.; Gaal, R.; Forro, L.; Hernadi, K. *Appl. Phys. Lett.* **2002**, *80*, 850.
(20) Blase, X.; Benedict, L. X.; Shirley, E. L.; Louie, S. G. *Phys. Rev. Lett.* **1994**, *72*, 1878.
(21) http://www.mercorp.com/.
(22) http://www.nanocyl.com/.
(23) The grids were purchased from Agar Scientific Company.
(24) Kilcoyne, A. L. D.; Tyliszczak, T.; Steele, W. F.; Fakra, S.; Hitchcock, P.; Franck, K.; Anderson, E. K.; Harteneck, B.; Rightor, E. G.; Mitchell, G.; Hitchcock, A. P.; Yang, L.; Warwick, T.; Ade, H. *J. Synchrotron Radiat.* **2003**, *10*, 125.
(25) Warwick, T.; Ade, H.; Kilcoyne, A. L. D.; Kritscher, M.; Tyliszczak, T.; Fakra, S.; Hitchcock, A. P.; Hitchcock, P.; Padmore, H. A. *J. Synchrotron Radiat.* **2002**, *9*, 254.
(26) Jacobsen, C.; Wirick, S.; Flynn, G.; Zimba, C. *J. Microsc.* **2000**, *197*, 173.
(27) aXis2000 is written in interactive data language (IDL). It is available free for noncommercial use from http://unicorn.mcmaster.ca/aXis2000.html.
(28) Abbas, M.; Wu, Z. Y.; Zhong, J.; Ibrahim, K.; Fiori, A.; Orlanducci, S.; Sessa, V.; Terranova, M. L.; Davoli, I. *Appl. Phys. Lett.* **2005**, *87*, 051923.
(29) Nikitin, A.; Ogasawara, H.; Mann, D.; Denecke, R.; Zhang, Z.; Dai, H.; Cho, K.; Nilsson, A. *Phys. Rev. Lett.* **2005**, *95*, 225507.
(30) Braun, A.; Huggins, F. E.; Shah, N.; Chen, Y.; Wirick, S.; Mun, S. B.; Jacobsen, C.; Huffman, G. P. *Carbon* **2005**, *43*, 117.
(31) Kuznetsova, A.; Popova, I.; Yates, J. T.; Bronikowski, M. J.; Huffman, C. B.; Liu, J.; Smalley, R. E.; Hwu, H. H.; Chen, J. G. *J. Am. Chem. Soc.* **2001**, *123*, 10699.
(32) Felten, A.; Hody, H.; Bittencourt, C.; Pireaux, J.-J.; Hernandez-Cruz, D.; Hitchcock, A. P. *Appl. Phys. Lett.* **2006**, *89*, 093123.
(33) Henke, B. L.; Gullikson, E. M.; Davis, J. C. *At. Data Nucl. Data Tables* **1993**, *54*, 181.
(34) Koprinarov, I. N.; Hitchcock, A. P.; McCrory, C. T.; Childs, R. F. *J. Phys. Chem. B* **2002**, *106*, 5358.
(35) Takekoh, R.; Okubo, M.; Araki, T.; Stover, H. D. H.; Hitchcock, A. P. *Macromolecules* **2005**, *38*, 542.
(36) Schiessling, J.; Kjeldgaard, L.; Rohmund, F.; Falk, L. K. L.; Campbell, E. E. B.; Nordgren, J.; Bruhwiler, P. A. *J. Phys.: Condens. Matter* **2003**, *15*, 6563.
(37) Shimada, T.; Yanase, H.; Morishita, K.; Hayashi, J.; Chiba, T. *Carbon* **2004**, *42*, 1635.
(38) Lawrence, J. R.; Swerhone, G. D. W.; Leppard, G. G.; Araki, T.; Zhang, X.; West, M. M.; Hitchcock, A. P. *Appl. Environ. Microbiol.* **2003**, *69*, 5543.
(39) Bluhm, H.; Andersson, K.; Araki, T.; Benzerara, K.; Brown, G. E.; Dynes, J. J.; Ghosal, S.; Gilles, M. K.; Hansen, H.-C.; Hemminger, J. C.; Hitchcock, A. P.; Ketteler, G.; Kilcoyne, A. L. D.; Kneedler, E.; Lawrence, J. R.; Leppard, G. G.; Majzlam, J.; Mun, B. S.; Myneni, S. C. B.; Nilsson, A.; Ogasawara, H.; Ogletree, D. F.; Pecher, K.; Salmeron, M.; Shuh, D. K.; Tonner, B.; Tyliszczak, T.; Warwick, T.; Yoon, T. H. *J. Electron Spectrosc. Relat. Phenom.* **2006**, *150*, 86.
(40) Dynes, J. J.; Tyliszczak, T.; Araki, T.; Lawrence, J. R.; Swerhone, G. D. W.; Leppard, G. G.; Hitchcock, A. P. *Environ. Sci. Technol.* **2006**, *40*, 1556.
(41) Dynes, J. J.; Lawrence, J. R.; Korber, D. R.; Swerhone, G. D. W.; Leppard, G. G.; Hitchcock, A. P. *Sci. Total Environ.* **2006**, *369*, 369.
(42) Hernández Cruz, D.; Hitchcock, A. P.; West, M. M.; Rousseau, M.-E.; Pézolet, M. *Biomacromolecules* **2006**, *7*, 836.

NL071134E